Volume 17
Number 8
24 February 2026
Pages 783-866

Polymer Chemistry

rsc.li/polymers

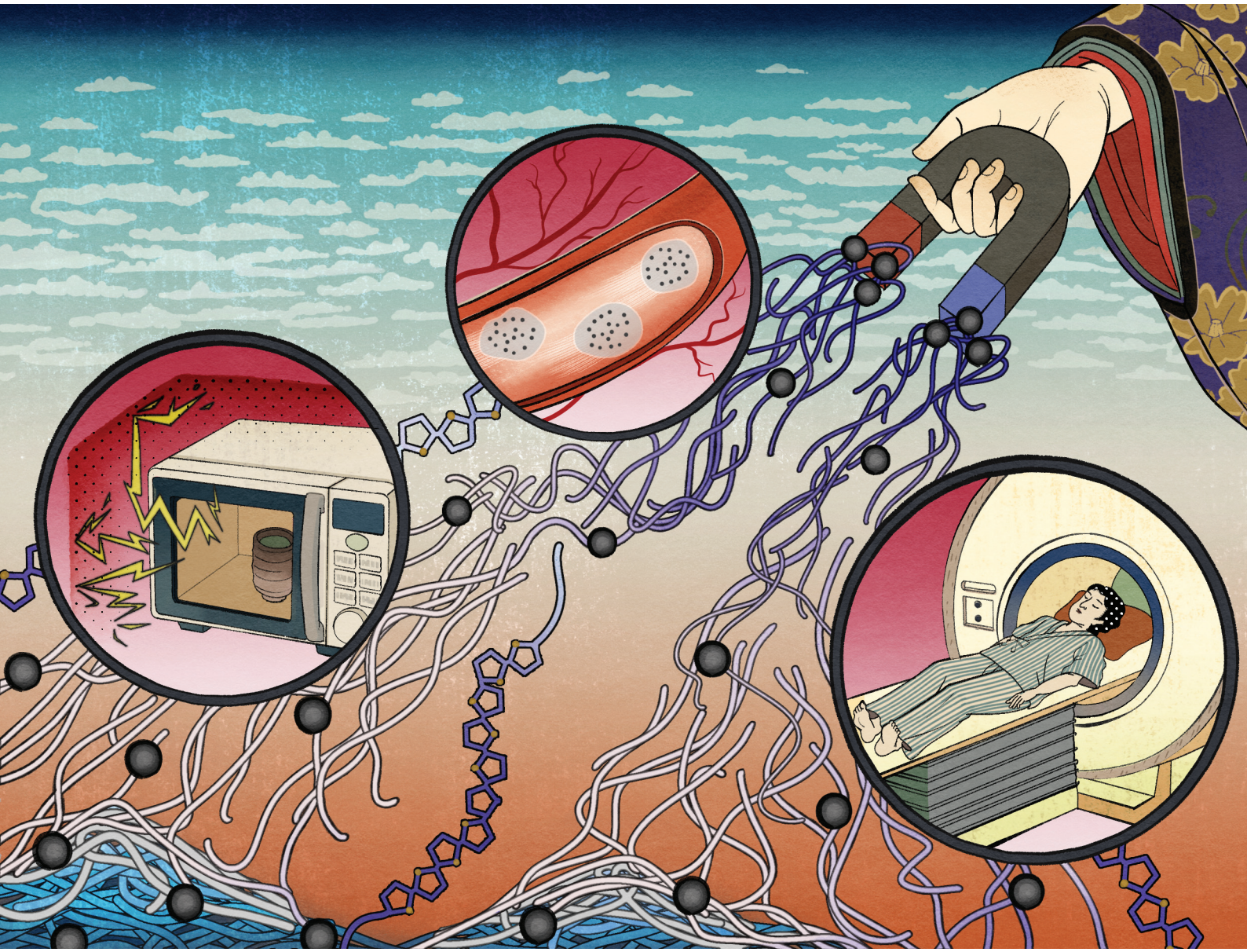

ISSN 1759-9962

ROYAL SOCIETY OF CHEMISTRY

PAPER

Katsuyoshi Hoshino, Satoru Tsukada *et al.*
Preparation, characterization, and magnetic properties of poly(3-methoxythiophene)-Fe_3O_4 conducting nanocomposite

Polymer Chemistry

ROYAL SOCIETY OF CHEMISTRY

PAPER

View Article Online
View Journal | View Issue

Cite this: *Polym. Chem.*, 2026, **17**, 796

Preparation, characterization, and magnetic properties of poly(3-methoxythiophene)-Fe_3O_4 conducting nanocomposite

Katsuyoshi Hoshino, *[a,b] Kiho Kashiwagi,[a] Minako Tachiki,[a] Hyuma Masu[b] and Satoru Tsukada *[a]

Conducting polymers complexed with magnetic nanoparticles have attracted considerable attention in recent years due to their potential applications in magnetic materials for biomedical and clinical uses. In this study, a unique and facile method is described for the preparation of a novel composite, which consists of poly(3-methoxythiophene) combined with Fe_3O_4 nanoparticles. Notably, hydrazine reduction of the resulting complex formed between poly(3-methoxythiophene) and the iron chlorides produced the desired composite under an ambient atmosphere without any additional energy input. This was also achieved without controlling the amount and addition rate of hydrazine, or adjusting the system pH. Elemental analysis, X-ray powder diffractometry, X-ray photoelectron spectroscopy, and Fourier-transform infrared spectroscopy indicated that the approximate empirical formula of the composite was $(C_5H_5OS)_2(C_5H_4OS)_{9.3}{\cdot}0.25Cl{\cdot}5.5Fe_3O_4{\cdot}9.4H_2O$. Additionally, transmission electron microscopy and scanning electron microscopy observations demonstrated the presence of almost spherical Fe_3O_4 particles with diameters ranging from ~20 to 200 nm in the composite. Furthermore, superconducting quantum interference device measurements demonstrated its superparamagnetic behavior with a saturation magnetization of 11.9 emu g^{-1} at 300 K. Moreover, ferrimagnetic behavior was detected, with a saturation magnetization of 20.2 emu g^{-1} and a coercivity of 500 Oe at 5 K. Overall, this work represents a novel and mild approach for the synthesis of magnetic materials using polythiophenes, one of the most prominent and commercially successful conducting polymers, which are known to exhibit good chemical and electrochemical stabilities under air, and in the presence of moisture, both in the doped and undoped states.

Received 24th September 2025,
Accepted 6th January 2026

DOI: 10.1039/d5py00933b

rsc.li/polymers

1. Introduction

The potential of magnetic responsive particles for application in mechanochemical, biomedical, and chemical research has led to extensive investigations in these fields.[1] By combining such magnetic particles with polymer materials, composite materials with excellent magnetic response properties can be obtained, including smart polymers for actuation, drug delivery, cell therapy, separation/concentration, and sorbent adsorption, among other functions.[2–8]

In the case where the polymeric materials are conducting polymers, their composites with magnetic nanoparticles will exhibit both electrical conduction and magnetism. Consequently, in addition to the aforementioned applications for composite materials consisting of insulating polymers and magnetic nanoparticles, multifunctional materials incorporating conducting polymers can be employed in the fabrication of batteries, electrochemical displays, sensors, electromagnetic shielding materials, microwave absorbing materials, and other devices. Indeed, numerous composite materials of conducting polymers and magnetic nanoparticles have been prepared. However, with the exception of a few revised or simplified methods,[9,10] such composites have been prepared primarily by solubilizing the precursor monomer of the conducting polymer in an aqueous micelle or emulsion medium with dispersed magnetic particles, and then chemically polymerizing the monomer using an oxidizing agent.[11–18] In the context of magnetic particles, Fe_3O_4 (magnetite) and γ-Fe_2O_3 (maghemite) have been widely employed in combination with conducting polymers such as polyaniline (PANI), polypyrrole (PPy), and poly(3,4-ethylenedioxythiophene) (PEDOT). Additionally, anionic sodium dodecyl sulfate and cationic cetyltrimethylammonium bromide have been employed as surfactants, while iron chlorides and ammonium persulfate have been used as

[a]*Department of Materials Sciences, Graduate School of Engineering, Chiba University, 1-33 Yayoi-cho, Inage-ku, Chiba 263-8522, Japan.*
E-mail: k_hoshino@faculty.chiba-u.jp
[b]*Center for Analytical Instrumentation, Chiba University, 1-33 Yayoi-cho, Inage-ku, Chiba 263-8522, Japan*

oxidizing agents for the polymerization of conducting polymer precursors.

Previously, our group reported the polymerization of 3-methoxythiophene with $FeCl_3$ to form a water-soluble 3-methoxythiophene-linked conducting polymer with a weight-averaged polymerization degree of 11.3, and it was found that the coating films of this polymer exhibited gold-like colors.[19,20] However, unreacted $FeCl_3$ and its corresponding reaction product $FeCl_2$ inevitably remained within the polymer systems. Repeated washings did not remove these iron chlorides, thereby suggesting the presence of strong interactions between the polymer skeleton and the iron chlorides, resulting in complex formation. Such residual iron chlorides are typically regarded as impurities in the polymer and are perceived negatively. However, it was hypothesized that reduction of the polymer–impurity complex could yield a novel composite with unique magnetic properties. This could offer a simple and facile method for composite synthesis that has not been previously reported.

In this study, reduction of the aforementioned polymer–iron chloride complex is performed using hydrazine to generate a polymer composite containing Fe_3O_4. The ability of this polymer composite to exhibit ferrimagnetism and superparamagnetism is evaluated. One key aspect of this novel approach is the immobilization of the Fe_3O_4 precursors (*i.e.*, $FeCl_3$ and $FeCl_2$) within the polymer skeleton, which could facilitate a uniform dispersion of the reaction product (Fe_3O_4) within the composite. More importantly, during the material conversion of iron chlorides to iron oxide, it is expected that such immobilization could eliminate the requirement for an additional energy input (*e.g.*, thermal and/or microwave energy), thereby enabling the reaction to proceed under ambient temperature and pressure conditions. Overall, the aim of this work is to present a novel method for the preparation of a new Fe_3O_4/poly(3-methoxythiophene) (P3MeOT) magnetic composite, along with its detailed characterization.

2. Experimental

2.1. Materials

3-Methoxythiophene (>98%) was purchased from FUJIFILM Wako Pure Chemical Corp. Anhydrous iron(III) chloride (>95%, FUJIFILM Wako Pure Chemical Corp.) and iron(III) perchlorate hydrate (anhydride content = 70.7%, FUJIFILM Wako Pure Chemical Corp.) were used as oxidizing agents for the polymerization of 3-methoxythiophene. Methanol (>99.8%), ethanol (>99.5%), and acetonitrile (>99.7%) were obtained from Kanto Chemical Co., Inc. Chemical de-doping was performed using hydrazine monohydrate (98%, Sigma-Aldrich).

2.2. Preparation of Cl-doped poly(3-methoxythiophene)

Chloride-doped poly(3-methoxythiophene), denoted P3MeOT-Cl, was prepared with reference to a previously reported method.[19,20] More specifically, to a stirred 0.10 M solution of 3-methoxythiophene in acetonitrile (20 mL) was added rapidly a 0.20 M solution of $FeCl_3$ in acetonitrile (20 mL) under a nitrogen atmosphere at 21 °C. The color of the solution changed rapidly from colorless to dark purple. The obtained purple solution was stirred for a further 2 h, followed by evaporation of the solvent. The obtained residue was repeatedly washed with ethanol to remove the oxidant and any remaining monomeric 3-methoxythiophene. More specifically, washing was continued until a clear wash solution was obtained. Subsequently, the residue was dried in a vacuum dryer (ETTAS AVO-250NB, AS ONE) at 50 °C for 90 min to yield the deep blue-purple P3MeOT-Cl (mass yield = 43%) with a weight-averaged polymerization degree of 11.3.[20] As described in the introduction, P3MeOT-Cl contains iron chlorides that cannot be removed by washing with ethanol.

2.3. Preparation of ClO_4-doped poly(3-methoxythiophene)

Poly(3-methoxythiophene) doped with the perchlorate anion (P3MeOT-ClO_4) was subsequently prepared according to previous literature methods.[21–23] In this case, to a stirred 0.10 M solution of 3-methoxythiophene in acetonitrile (20 mL) was added rapidly a 0.20 M solution of $Fe(ClO_4)_3$ in acetonitrile (20 mL) under a nitrogen atmosphere at 22 °C. The color of this solution changed rapidly from transparent/colorless to dark blue. The obtained solution was stirred for 2 h, and the dark blue precipitate was isolated by suction filtration. After washing the resulting product five times with methanol, it was dried at 50 °C under vacuum for 90 min to give the desired P3MeOT-ClO_4 as a deep blue powder (mass yield = 96%) with a weight-averaged polymerization degree of 20.4.[19] Unlike the above-described P3MeOT-Cl, P3MeOT-ClO_4 does not contain the iron component derived from the oxidant used during the polymerization process.[21] Additionally, the prepared P3MeOT-ClO_4 is soluble in polar organic solvents, such as nitromethane, propylene carbonate, γ-butyrolactone, and acetonitrile, and its solution-cast films exhibit a gold-like luster.

2.4. Synthesis of the reduced form of P3MeOT-Cl

The reduced form of P3MeOT-Cl (Red 1) was prepared following a previously described literature method.[23] More specifically, P3MeOT-Cl (0.10 g) and hydrazine monohydrate (10 mL) were placed in an eggplant flask and stirred for 5 h. Subsequently, suction filtration was performed using a glass filter and a membrane filter (maximum pore size: 0.1 μm), followed by repeated washing with ethanol. The residue was subsequently dried at 50 °C under vacuum for 90 min, yielding Red 1 as a black solid (mass yield = 25%).

2.5. Synthesis of the reduced form of P3MeOT-ClO_4

The reduced form of P3MeOT-ClO_4 (Red 2) was prepared in the same manner as Red 1, following the same literature procedure[23] to obtain Red 2 as a deep purple solid. As described later (subsection 3.4), Red 2 serves as a suitable reference material for Red 1.

2.6. General instrumentation and analytical methods

Morphological observations were performed using scanning electron microscopy (SEM; JSM-6510A, JEOL) and transmission electron microscopy (TEM; H-7650, Hitachi High-

Technologies). Energy dispersive X-ray (EDX) spectroscopy combined with SEM (JED-2300 detector, JEOL) and TEM (rTEM detector, AMETEK) were used to evaluate the elemental compositions of the prepared materials and to record their corresponding element mapping images, respectively. For the purpose of SEM imaging, the samples were placed on conductive tape and fixed onto the sample stage. To prepare the TEM samples, polymer suspensions were prepared by adding ethanol and the desired polymer (0.1 wt%) to a glass vial, followed by ultrasonic dispersion for 20 min. A copper grid (STEM Cu150P, Okenshoji) was then placed on a cleaned glass slide with the front side facing upward, and a drop of the prepared suspension was applied onto the grid. The sample was subsequently dried in a vacuum dryer at 25 °C for 24 h to obtain the TEM specimen. X-ray powder diffractometry (XRD) was performed using a Bruker D8 Advance instrument (Bruker AXS) equipped with a Cu-Kα radiation source (λ = 1.54056 Å, 40 kV, 40 mA). X-ray photoelectron spectroscopy (XPS) was carried out using a photoelectron spectrometer (JPS-9030, JEOL) with Mg-Kα radiation (1253.6 eV), wherein the absolute binding energy scale was determined by setting the C 1s signal to 284.6 eV. The Fourier-transform infrared (FT-IR) transmission spectra of the polymers were recorded using a Jasco FT/IR-410 spectrometer. The FT-IR samples were prepared by placing the polymer powders between two mini KBr plates (Jasco) and applying pressure using a Jasco mini hand press (MP-1). Elemental analysis was performed for carbon and hydrogen on an Exter Analytical CE-440 instrument, and for sulfur and chlorine on a System Instruments NS-11 device coupled with an ion chromatograph (IC-2010, TOSOH). Magnetization measurements were carried out using a superconducting quantum interference device (SQUID) magnetometer (Quantum Design MPMS) at 5 and 300 K.

3. Results and discussion

3.1. Magnetism demonstrations for P3MeOT-Cl and Red 1

Fig. 1 shows the behaviors of P3MeOT-Cl and Red 1 when brought close to a ferrite magnet. While P3MeOT-Cl did not adhere to the magnet (Fig. 1a), Red 1 exhibited complete attachment (Fig. 1b), thereby demonstrating that Red 1 possesses magnetic properties.

3.2. SEM-EDX measurements

SEM observations of P3MeOT-Cl and Red 1 were conducted, and the corresponding images are shown in Fig. 2. Notably, Red 1 was found to consist of an aggregate of bulk particles, whereas P3MeOT-Cl showed partially separated and dispersed aggregates, with ribbon-like particle morphologies also being observed. Such separation of the particle aggregates due to doping has also been reported for other polythiophenes,[24] and is likely caused by doping-induced structural transformations or an increase in the polymer crystallinity.[25] The comprehensive microstructural characteristics and corresponding EDX spectra are provided in the SI (Fig. S5).

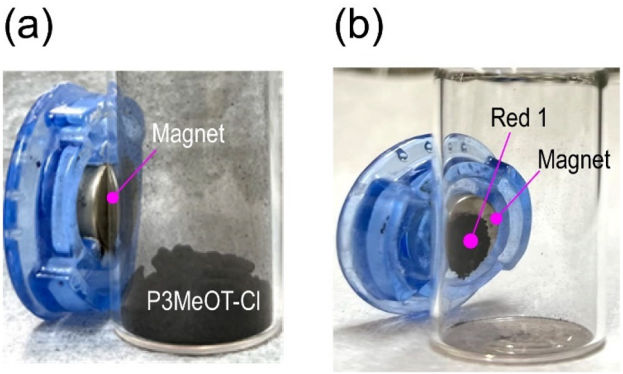

Fig. 1 Photographic images showing the behaviors of (a) P3MeOT-Cl and (b) Red 1 when brought close to a magnet through a glass vial. The black circular magnet is located at the center of the blue plastic support. The diameter of the glass vial is 20 mm.

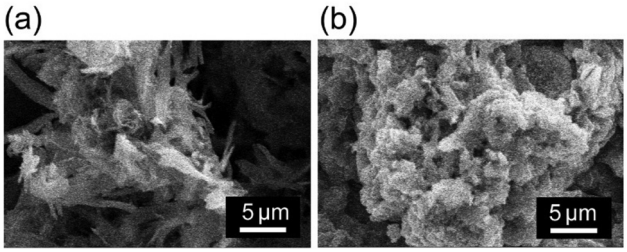

Fig. 2 SEM images recorded for (a) P3MeOT-Cl and (b) Red 1.

Table 1 presents the EDX results for P3MeOT-Cl and Red 1, showing the atomic ratios of S, Cl, Fe, and O in each sample. For clarity, the atomic ratios of Cl, Fe, and O were normalized to an atomic concentration of 1 for S. According to previous literature,[20] the Fe detected in P3MeOT-Cl originates from a mixture of $FeCl_3$ and $FeCl_2$, wherein the latter is a byproduct that is produced during the synthesis of P3MeOT-Cl. Previous rigorous analysis demonstrated that $FeCl_3$ and $FeCl_2$ exist in a molar ratio of 2 : 3.[20] Additionally, Table 1 indicates that the Fe/S ratio is higher in Red 1 (Fe/S = 1.47) than in P3MeOT-Cl (Fe/S = 0.27). This difference is likely due to the fact that during the filtration and washing processes performed following the reduction of P3MeOT-Cl to produce Red 1 (see subsection 2.4), almost 70% of the polymer components in the product dissolved in the filtrate and were lost. In contrast, the iron-containing polymer components did not dissolve, and

Table 1 Atomic ratios of Cl, Fe, and O relative to S in the P3MeOT-Cl and Red 1 molecules[a]

Molecule	S	Cl	Fe	O
P3MeOT-Cl	1.00	0.83	0.27	1.00
Red 1	1.00	0.022	1.47	5.79

[a] Atomic ratios were obtained by EDX measurements and normalized to S.

were almost entirely recovered, thereby resulting in an increased Fe/S ratio.

With regards to the Cl content, the Cl present in P3MeOT-Cl represents the sum of the Cl derived from the aforementioned iron chlorides ($FeCl_3$ and $FeCl_2$) and the Cl^- doped into the P3MeOT structure. The ratio of doped Cl^- per 3-methoxythiophene unit is defined as the doping level. As detailed in the table, a larger Cl/S ratio was obtained for P3MeOT-Cl than for Red 1 because of the inclusion of iron chlorides ($FeCl_3$ and $FeCl_2$). Whereas, the Cl/S ratio obtained for Red 1 was extremely small, indicating that Cl^- de-doping occurs during the reduction reaction performed in the presence of hydrazine.

Focusing next on the O content, a significantly higher O abundance was detected in Red 1 than in P3MeOT-Cl. Notably, the O component of P3MeOT-Cl corresponds to the oxygen present in the P3MeOT framework, as indicated by the equal ratio of S to O. On the other hand, the content of O in Red 1 is considerably higher than the S content, suggesting that a portion of its O fraction originates from sources other than the framework.

3.3. TEM-EDX measurements

Subsequently, TEM observations were conducted for P3MeOT-Cl and Red 1, as shown in Fig. 3. More specifically, Fig. 3a and b show the images recorded for two different batches of P3MeOT-Cl, while Fig. 3c presents a magnified view of the sample shown in Fig. 3b. As observed in Fig. 2a, P3MeOT-Cl exhibits a ribbon-like morphology, with almost no contrast being observed within the images. Similarly, Fig. 3d and e show the images obtained for two different batches of Red 1, and Fig. 3f is a magnified view of Fig. 3e, where clear contrast can be observed. The dark regions were assumed to correspond to areas containing high concentrations of Fe (a heavy element), namely the iron compound formed upon hydrazine reduction of the iron chlorides. On the other hand, although P3MeOT-Cl contains iron chlorides, which also include the heavy element Fe, the lack of contrast observed in its TEM images was attributed to a uniform distribution of these species within the sample. In addition, the proportion of dark regions in Red 1 is relatively high, which is consistent with the high Fe/S ratio detailed in Table 1. Furthermore, these dark regions consist of rounded particles with sizes ranging from several nanometers up to ~200 nm, which are distributed throughout the sample with little spatial bias. To further investigate these rounded particle structures, elemental mapping was performed.

The results of the elemental mapping analysis are presented in Fig. 4. From these results, it was confirmed that Fe originates from the iron product generated during the hydrazine reduction protocol, O is derived from P3MeOT and the reduction product, while S and C originate from P3MeOT. These elements were found to be clearly distributed throughout the sample. More specifically, Fe and O were strongly mapped in the contrast regions observed in Fig. 3d, whereas S was predominantly mapped in areas outside the contrast

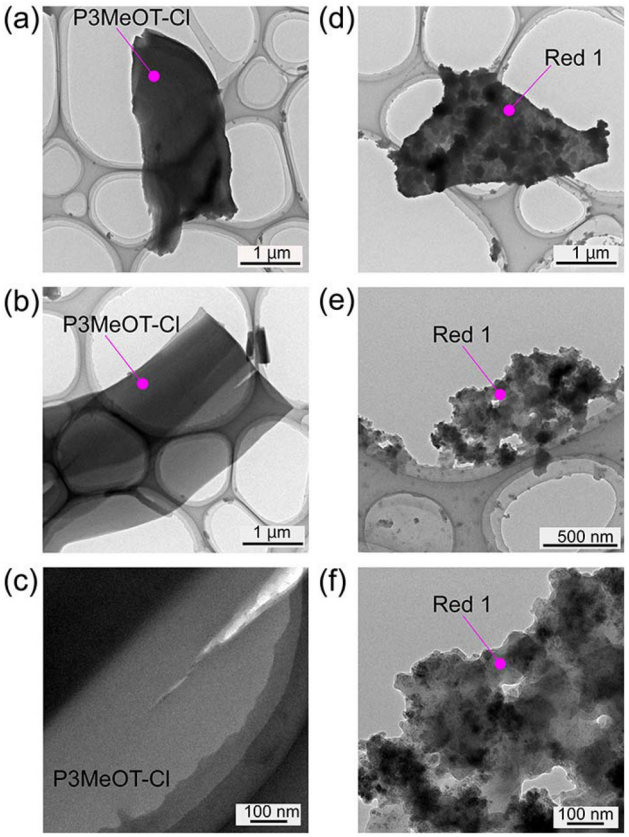

Fig. 3 TEM images of (a–c) P3MeOT-Cl and (d–f) Red 1. The mesh-like structures visible in the backgrounds of the images correspond to the supporting membranes on the copper grids used during the TEM observations.

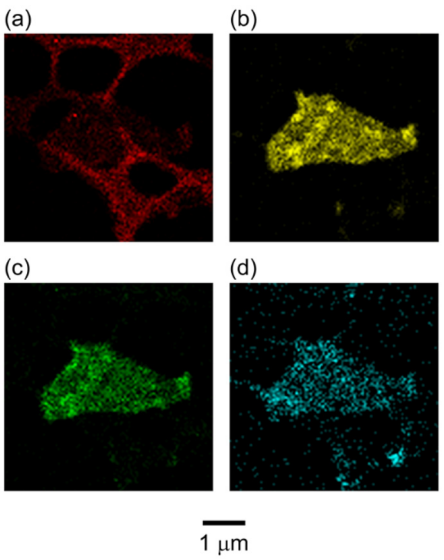

Fig. 4 EDX elemental mapping images recorded for the (a) C, (b) Fe, (c) O, and (d) S components of Red 1. Mapping was performed based on the TEM image shown in Fig. 3d.

regions. These findings confirm that Red 1 is a composite of P3MeOT and the reduction product, thereby supporting the results described in subsection 3.2. The elemental maps for P3MeOT-Cl are presented in Fig. S1 in SI.

3.4. XRD measurements

To identify the hydrazine reduction products present in Red 1, XRD measurements were performed for both Red 1 and Red 2, as shown in Fig. 5. Notably, the EDX results (Table S1, SI) indicated that neither Red 2 nor its precursor P3MeOT-ClO_4 contained Fe components derived from the oxidizing agent. Therefore, Red 2 can be considered to consist solely of P3MeOT, thereby rendering it an appropriate reference sample for comparison with Red 1. Given that these compounds are largely devoid of iron compounds, the presence of magnetism attributable to the reduced products is not anticipated. Furthermore, neither the P3MeOT framework (Red 2) nor its perchlorate ion-doped counterpart (P3MeOT-ClO_4) exhibited significant magnetic properties (Figs. S6 and S7, SI), suggesting that any intrinsic magnetism within the framework is negligible. Consequently, it is inferred that these compounds did not adhere to the magnet because of the absence of components exhibiting notable magnetic characteristics (Fig. S2, SI). In terms of the XRD results, Red 1 exhibited peaks at 2θ values of 18.2, 30.7, 35.6, 43.2, 57.0, and 62.5°, which correspond with the 111, 220, 311, 400, 511, and 440 reflections of the Fe_3O_4 nanoparticles, respectively (JCPDS database, file no. 19-0629).[14,16–18] The average crystallite size of the hydrazine reduction product, d, can be estimated from the Scherrer equation:

$$d = \kappa\lambda/\beta \cos\theta$$

where λ is the X-ray wavelength, κ is the shape factor, θ is the Bragg angle in radians, and β is the full width at half maximum in radians. If the shape of the crystal is unknown, κ is often taken as 0.89.[17,18] Thus, for the most distinct reflecting peak at a 2θ value of 35.6°, the d value was calculated to be 7.6 nm. Notably, this value was obtained under the assumption that the diffraction peak width is solely attributed to the crystallite size, without accounting for the influences imparted by other factors. The obtained value therefore represents the lower limit of the crystallite size. Additionally, in the XRD spectrum of Red 2, the main peaks were observed at 2θ values of 13.2 and 25.0° (Fig. 5b), both of which originate from P3MeOT, and these signals were also observed in the spectrum of Red 1 (Fig. 5a). These results suggest that Red 1 is likely composed of Fe_3O_4 and P3MeOT. However, since γ-Fe_2O_3 has also been reported to show signals at 2θ values close to those of Fe_3O_4,[13,16] distinguishing between these two substances by XRD measurements is challenging.[26] Thus, XPS was subsequently employed to differentiate between Fe_3O_4 and γ-Fe_2O_3, as detailed below.[27]

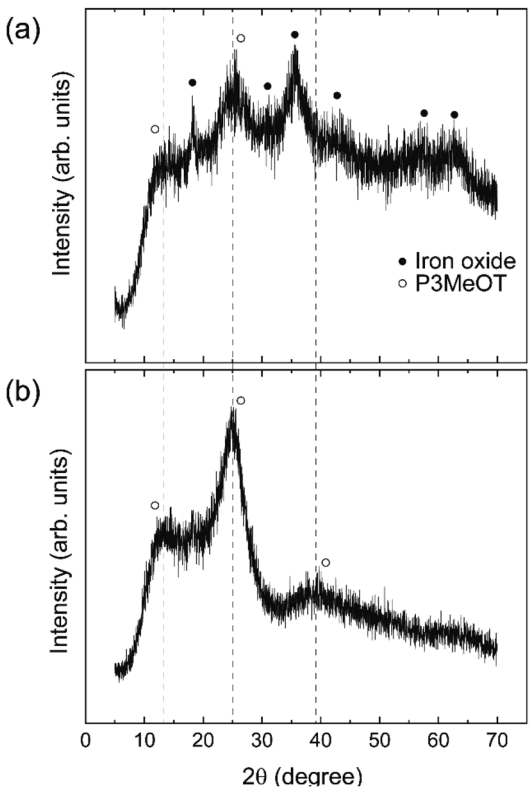

Fig. 5 XRD patterns recorded for (a) Red 1 and (b) Red 2.

3.5. XPS measurements

From the results of the previous subsection, it was determined that the hydrazine reduction product contained in Red 1 originates from an iron oxide (either Fe_3O_4 or Fe_2O_3), which is derived from the iron chlorides present in P3MeOT-Cl. Thus, to identify the iron oxide species, XPS measurements were performed on both P3MeOT-Cl and Red 1, as presented in Fig. 6.

More specifically, Fig. 6 shows the XPS spectra recorded for the Fe $2p_{3/2}$, O 1s, and Cl 2p components of P3MeOT-Cl and Red 1. In the Fe $2p_{3/2}$ spectrum of P3MeOT-Cl, a peak was observed at a binding energy of 709.8 eV. However, according to previous literature,[28] $FeCl_3$ and $FeCl_2$ are expected to exhibit peaks at 711.5 and 710.8 eV, respectively. More specifically, Hatfield *et al.*[28] previously measured the XPS spectra of $FeCl_3$, $FeCl_2$, and $(TTF)_2FeCl_3$ (TTF = tetrathiafulvalene), and reported incomplete charge transfer from the TTF donor to iron in the $(TTF)_2FeCl_3$ system due to the fact that the binding energy of the core Fe $2p_{3/2}$ electrons in $(TTF)_2FeCl_3$ is smaller than those in $FeCl_3$ and $FeCl_2$.[28] Hence, the above result indicates the presence of a greater electron density on the Fe components of $FeCl_3$ and $FeCl_2$ attached to P3MeOT-Cl (*cf.*, those in the free $FeCl_3$ and $FeCl_2$ species). This suggests that partial electron transfer occurs from P3MeOT to $FeCl_3$ and $FeCl_2$. Importantly, this implies the presence of interactions between the iron chlorides and the P3MeOT skeleton, consistent with the observation that iron chlorides were not removed by rigorous washing procedures during the synthetic process (see subsection 2.2).

Additionally, the Fe $2p_{3/2}$ spectrum of Red 1 exhibited a peak at 709.5 eV, consistent with the presence of Fe_3O_4 (Fe_3O_4:

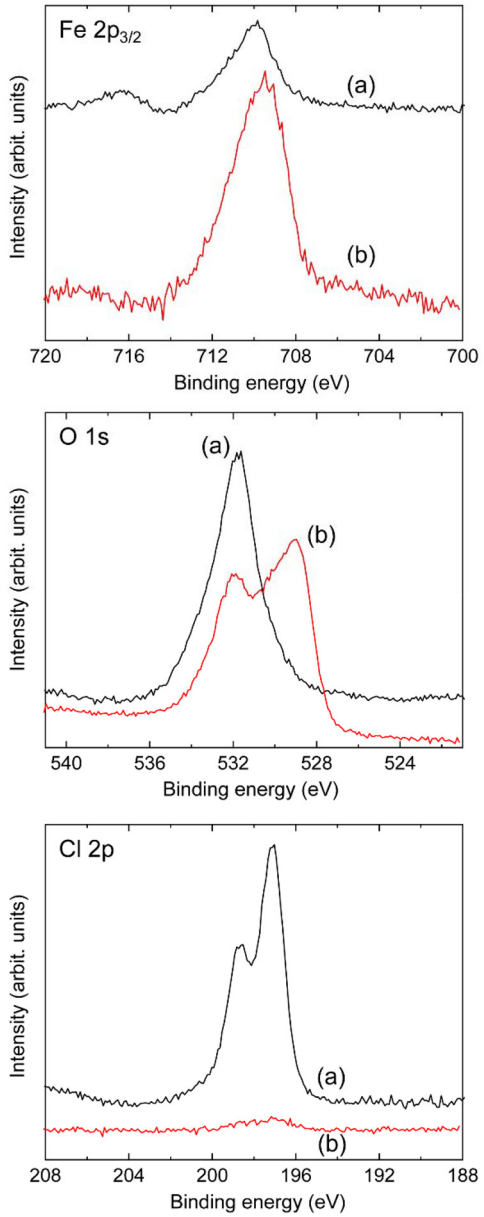

Fig. 6 XPS spectra recorded for Fe $2p_{3/2}$ (top), O 1s (middle), and Cl 2p (bottom) for (a) P3MeOT-Cl and (b) Red 1.

707.9–710.2 eV,[29–32] Fe_2O_3: 710.3–710.8 eV[29,30,33,34]). Additionally, the magnitude of the Fe^{3+} shake-up satellite signal[35] originating from Fe_2O_3 (*i.e.*, at ~718 eV) was found to be negligibly small compared to that of the Fe $2p_{3/2}$ peak, further supporting the conclusion that the iron compound in this system is Fe_3O_4. Although metallic iron exhibits a peak in the range of 706.50–707.50 eV,[29,30,36] the absence of such a signal in the spectrum of Red 1 indicates that metallic iron is not present.

In the O 1s spectrum, recorded for P3MeOT-Cl, a peak was observed at 531.6 eV. Considering that a similar peak was also observed for P3MeOT-ClO_4 (*i.e.*, at 531.7 eV, Fig. S3, SI), this was attributed to the methoxy oxygen atom of the P3MeOT framework. Notably, in addition to a signal at 531.7 eV, the O 1s spectrum recorded for Red 1 exhibited an additional peak at 529.1 eV. Considering that the oxygen components of Fe_3O_4 and Fe_2O_3 exhibit peaks in the ranges of 528.9–529.8 eV[29,30,37] and 529.6–531.8 eV,[29,30,33,34,38,39] respectively, the peak at 529.1 eV was considered to originate from Fe_3O_4. Therefore, based on the above series of results, the iron oxide contained in Red 1 was determined to be Fe_3O_4.

Moreover, the Cl 2p spectrum recorded for P3MeOT-Cl exhibited signals at 198.6 and 197.0 eV, which correspond to the $2p_{1/2}$ and $2p_{3/2}$ states of Cl, respectively.[40] Consequently, these signals were attributed to the doped Cl^- species in P3MeOT-Cl and the Cl^- components of the impurity iron chlorides. Considering previous literature,[40] the absence of binding energy shifts for the Cl signals of the iron chlorides indicates that interactions between the iron chlorides and the P3MeOT framework occurred at the Fe sites, rather than at the Cl sites. On the other hand, in spectrum recorded for Red 1, the Cl 2p signal almost disappeared, indicating that very low quantities of Cl exist in Red 1. This suggests that the hydrazine reduction of P3MeOT-Cl resulted in the almost complete de-doping of Cl^-, along with the near-complete conversion of the iron chloride impurities into Fe_3O_4.

As previously reported, Fe_3O_4 nanoparticles can be prepared *via* the hydrazine reduction of Fe^{3+} ions using microwave heating at elevated temperatures.[26,41,42] In such systems, Fe^{3+} ions are reduced to Fe^{2+} ions by hydrazine in the presence of oxygen. The Fe^{2+} ions are then combined with dissolved oxygen and hydroxyl ions to form γ-FeOOH, which then reacts with Fe^{2+} ions to form Fe_3O_4. In this approach, the phase and morphology of the resulting iron oxide particles are affected by the quantity and addition rate of hydrazine, as well as the pH of the precursor solution.[43] The current method is similar to this approach in that it uses hydrazine; however, it does not require heating, control of the hydrazine addition conditions, and adjustment of the solution pH. Although this is merely speculative, the XPS results suggest that the iron chlorides appear to be immobilized, while the Fe^{3+} ions present in these iron chlorides may be partially reduced through their interactions with the P3MeOT framework. Such partial reduction would likely promote the formation of Fe^{2+} ions through the action of hydrazine, thereby promoting the formation of Fe_3O_4, and eliminating any requirement to adjust the reaction conditions. The activation of iron chlorides by P3MeOT is of particular interest as it is analogous to the activation of dinitrogen by metal oxide photocatalysts, wherein dinitrogen is partially reduced at the oxygen vacancy sites of the photocatalysts, thereby allowing the thermodynamically challenging dinitrogen fixation reaction to occur.[44]

3.6. FT-IR spectroscopy

In a previous study, Deng *et al.*[17] fabricated a core–shell structure composed of Fe_3O_4 and polypyrrole (PPy). In the resulting FT-IR spectrum, the disappearance of a characteristic signal corresponding to PPy suggested an interaction between the lone pair of N electrons in the PPy chain and the 3d orbital of

the Fe atom in Fe_3O_4. Additionally, Singh *et al.*[15] suggested the formation Fe–S linkages based on the FT-IR spectrum recorded for a composite that had been prepared from γ-Fe_2O_3 and PEDOT. More specifically, this was implied by the disappearance of a characteristic signal corresponding to an Fe–O bond of γ-Fe_2O_3. Therefore, FT-IR measurements were also conducted herein to investigate the possible interactions between Fe_3O_4 and P3MeOT in Red 1, and to reconfirm the presence of Fe_3O_4 (Fig. 7).

Based on the spectra, the peaks observed at 1508 and 1518 cm^{-1} for P3MeOT-Cl and Red 1, respectively, were assigned to the stretching mode of the aromatic C=C bond for the inner thiophene rings.[45,46] Additionally, signals corresponding to $-CH_3$ bending were observed at 1432 and 1356 cm^{-1} in both spectra,[47] while the peaks detected at 1263 and 1252 cm^{-1} were assigned to the C–O–C stretching vibrations of the P3MeOT-Cl and Red 1 methoxy groups, respectively.[46] Furthermore, the signals observed at ~1210 cm^{-1} in both spectra correspond to stretching of the C–C inter-ring bonds,[48] while the peaks detected at 1061 and 1065 cm^{-1} for P3MeOT-Cl and Red 1, respectively, were attributable to C_β–H in-plane bending.[46,48]

Moreover, both spectra exhibited a band at 821 cm^{-1} which was assigned to the C–H deformation vibration of the 2,3,5-trisubstituted thiophene ring.[47,49] The bands observed at ~440 and 600 cm^{-1} in the spectrum of Red 1 were assigned to the vibrations of the octahedral and tetrahedral Fe–O bonds of Fe_3O_4, respectively,[10,50–53] thereby reconfirming that the iron oxide species in Red 1 is Fe_3O_4. It should also be noted that the peak observed at 1628 cm^{-1} for Red 1 is due to the O–H stretching vibrations of water (see subsection 3.7).[53] Overall, the obtained characterization results reveal that Red 1 is a composite of de-doped P3MeOT and Fe_3O_4. However, upon comparing the spectra recorded for P3MeOT-Cl and Red 1, no signal loss arising from the incorporation of Fe_3O_4 into P3MeOT was observed, and no evidence of interactions between the P3MeOT framework and Fe_3O_4 was obtained from the FT-IR data.

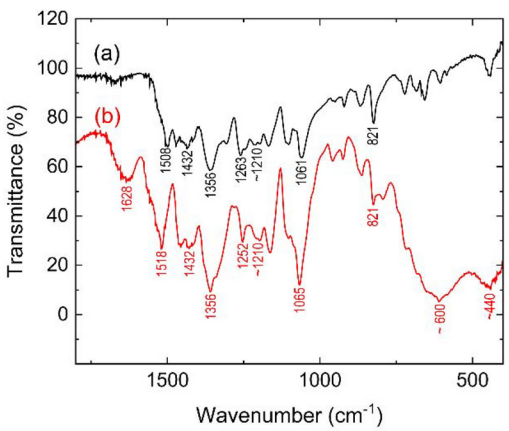

Fig. 7 FT-IR spectra recorded for (a) P3MeOT-Cl and (b) Red 1.

3.7. Elemental analysis

Subsequently, the chemical compositions of P3MeOT-Cl and Red 1 were estimated through elemental analysis. In the case of P3MeOT-Cl, previous SEM-EDX measurements performed on a solution-cast film region containing iron chloride impurities (*i.e.*, $FeCl_3$ and $FeCl_2$) revealed that a S/Cl/Fe composition ratio of 1 : 1.57 : 0.53.[20] Thus, considering that the Cl/S ratio in P3MeOT is 0.29 (*i.e.*, doping level = 29%),[19,20] the ratio of Cl derived from the iron chloride impurities was calculated to be 1.57–0.29 = 1.28. Therefore, the Fe/Cl ratio of the iron chlorides was determined to be 0.53 : 1.28 (*i.e.*, 1 : 2.4), ultimately giving an $FeCl_3$/$FeCl_2$ molar ratio of 2 : 3. Based on this result, along with the average degree of polymerization of P3MeOT (*i.e.*, 11.3),[19] the doping level of Cl^- (*i.e.*, 29%), and the potential presence of water,[21] the empirical formula of P3MeOT-Cl was assumed to be $(C_5H_5OS)_2(C_5H_4OS)_{9.3}{\cdot}3.2Cl{\cdot}xFeCl_3{\cdot}1.5xFeCl_2{\cdot}yH_2O$. In this formula, $(C_5H_5OS)_2$ represents the two thiophene units at the molecular termini, $(C_5H_4OS)_{9.2}$ refers to the linked thiophene units (excluding the terminal units), and x and y are coefficients. Table 2 provides a summary of the elemental analysis results obtained for P3MeOT-Cl and Red 1.

Thus, based on the elemental analysis data obtained for P3MeOT-Cl, the coefficients x and y were calculated to be 1.19 and 0.43, respectively, giving an empirical formula of $(C_5H_5OS)_2(C_5H_4OS)_{9.3}{\cdot}3.3C{\cdot}1.2FeCl_3{\cdot}1.8FeCl_2{\cdot}0.35H_2O$. Consequently, the molecular weight was calculated as 1.8×10^3, and the content of iron chlorides was determined to be 23 wt%. From this formula, the Fe/S ratio was determined to be 0.27, which agrees with that obtained from the EDX measurements, 0.27 (see Table 1).

In the case of Red 1, assuming that this species contains Fe_3O_4, water, and Cl (as indicated by the analyses presented in subsections 3.4 to 3.6), the empirical formula of Red 1 can be expressed as $(C_5H_5OS)_2(C_5H_4OS)_{9.3}{\cdot}pCl{\cdot}qFe_3O_4{\cdot}rH_2O$, where p, q, and r are coefficients. Similar to the case of P3MeOT-Cl, determining the coefficients p, q, and r from the data presented in Table 2 yielded values of 0.25, 5.5, and 9.4, respectively. Therefore, the empirical formula was defined as $(C_5H_5OS)_2(C_5H_4OS)_{9.3}{\cdot}0.25Cl{\cdot}5.5Fe_3O_4{\cdot}9.4H_2O$, thereby giving a molecular weight of 2.7×10^3. Furthermore, the Fe_3O_4 content was determined to be 47 wt%, indicating that approximately one Fe_3O_4 unit is incorporated into the molecule for every two thiophene units. The Fe/S ratio was calculated as 1.46, consistent with the value of 1.47 obtained from the EDX measurements (Table 1). Furthermore, the remarkably low atomic concentration of Cl suggests that both the de-doping of Cl^- *via* hydrazine reduction and the material conversion from iron chlorides

Table 2 Atomic ratios of the constituent elements of P3MeOT-Cl and Red 1, as determined by elemental analysis

Molecule	C (atom%)	H (atom%)	S (atom%)	Cl (atom%)
P3MeOT-Cl	37.39	2.66	20.31	21.04
Red 1	24.86	2.43	14.50	0.30

to Fe_3O_4 proceeded efficiently. As evidenced by Fig. S4 and S5 in SI, neither P3MeOT-Cl nor Red contain nitrogen.

In general, when conducting polymers are synthesized *via* chemical oxidation methods, structural defects and impurities are detected,[54] and the molecular weight distribution is not monodisperse. In fact, the polydispersity index of P3MeOT-Cl has previously been defined as 1.3.[20] As discussed in subsection 3.5, Cl is present only in trace amounts in Red 1, and so the Cl content of Red 1 shown in Table 1 falls within the margin of error for elemental analysis. Given these considerations, the empirical formulae determined for P3MeOT-Cl and Red 1 should be regarded as approximate representations rather than definitive compositions.

3.8. Magnetic property measurements

Based on the results described in previous subsections 3.2 to 3.7, it was revealed that Red 1 is a composite of P3MeOT and Fe_3O_4. Fe_3O_4 is known to exhibit ferrimagnetism, whereas the P3MeOT backbone (equivalent to Red 2) does not (Fig. S6 in SI). Consequently, the magnetism exhibited by Red 1 in Fig. 1b can be ascribed to the presence of Fe_3O_4. With these considerations in mind, the magnetic properties of Red 1 were subsequently measured using a SQUID. Fig. 8a and b show the magnetic hysteresis loops of Red 1 measured at 5 K and its magnification close the origin, respectively. More specifically, the hysteresis loop shown in Fig. 8a exhibits a saturation magnetization, M_s, of 20.2 emu g^{-1} under a magnetic field of 50 kOe, while a remanence of 3.1 emu g^{-1} and a coercivity of 500 Oe were obtained from that shown in Fig. 8b. This behavior indicates that Red 1 is ferrimagnetic at 5 K. Additionally, the hysteresis loop obtained at 300 K exhibits an M_s value of 11.9 emu g^{-1} under a magnetic field of 50 kOe (Fig. 8c), and the absence of coercivity and remanence (Fig. 8d) indicates that Red 1 is superparamagnetic, *i.e.*, it is attracted by an external magnetic field, but does not retain any magnetism once the external field is removed. The development of this superparamagnetic nature can be attributed to the small nano-sized Fe_3O_4 particles present in Red 1. In such nanoparticles, a single magnetic domain may be formed where the energy barrier for spin reversal is easily overcome by thermal vibrations, thereby resulting in superparamagnetism.[51] Moreover, the M_s value of Red 1 (11.9 emu g^{-1} at 300 K) was found to be smaller than that of the Fe_3O_4 nanoparticles (46.7 emu g^{-1} at room temperature),[55] partly due to the lower weight ratio of Fe_3O_4 nanoparticles in Red 1 compared with the Fe_3O_4 nanoparticles alone.[14,18] However, even when taking into account the weight ratio of Fe_3O_4 in Red 1 (see subsection 3.7), the M_s value for Red 1 remains unequal to that for the Fe_3O_4 nanoparticles alone. By analogy with previous reports, this could be attributed to the P3MeOT coating influencing the surface spins of the Fe_3O_4 nanoparticles. More specifically, Wei *et al.*[52] demonstrated that the M_s value of Fe_3O_4 nanoparticles decreases upon modification with sodium citrate and oleic acid. They attributed this result to the surface spin effect on the Fe_3O_4 nanoparticles caused by the modification. Similarly, Si *et al.*[56] reported that a smaller M_s value was obtained for a composite of Fe_3O_4 nanoparticles and surfactants compared to that of a commercial Fe_3O_4-based magnetic fluid. They suggested that this effect was caused by the influence of the surfactants on the surface spins of the Fe_3O_4 nanoparticles.

Thus, as evidenced both by the findings of the current study and by prior reports, the magnetization of magnetic nanoparticles is generally reduced due to organic coatings. However, such coatings play a crucial role in the fields of medicine and biology. For instance, in drug delivery applications, polymer coatings enhance the biocompatibility and stability of magnetic nanoparticles in the bloodstream.[57] In the case of magnetic resonance imaging (MRI) contrast agents, coatings contribute to improved dispersibility and prolonged circulation time of the particles *in vivo*.[58] Furthermore, in biosensing and bioseparation, coated magnetic particles can be engineered to specifically bind to particular biomarkers or cell surface molecules.[59]

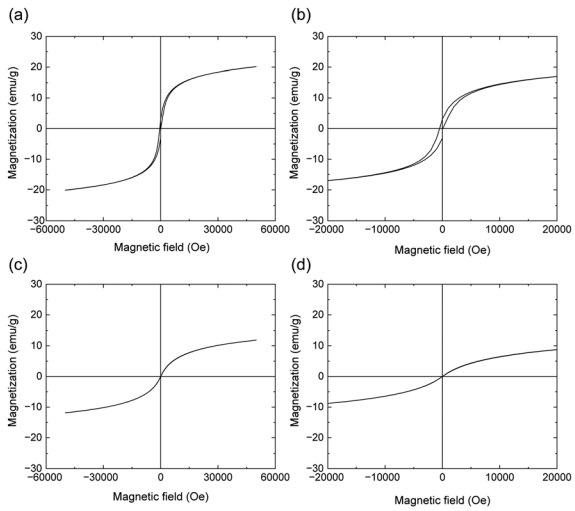

Fig. 8 Magnetic hysteresis loops recorded for Red 1 at (a, b) 5 K and (c, d) 300 K. The loops shown in panels (b) and (d) represent magnifications of the origin regions shown in panels (a) and (c), respectively.

4. Conclusions

In this study, a novel method for the synthesis of a superparamagnetic nanocomposite of poly(3-methoxythiophene) (P3MeOT) and Fe_3O_4 was described. The composite was prepared *via* a simple reaction between P3MeOT-Cl and hydrazine in the presence of oxygen at an ambient temperature and pressure. This straightforward approach was characterized by the fact that no additional energy input was required, and control of the amount or addition rate of hydrazine was not necessary, nor was adjustment of the solution pH. Notably, such controls are generally required in the hydrazine-driven reduction method for the conversion of Fe^{3+} ions to Fe_3O_4. Based on experimental findings, the characteristics of the described reaction were discussed in the context of the elec-

tronic interactions between P3MeOT and the iron chlorides, and the presumed activation of iron chlorides resulting from these interactions were considered.

Polythiophenes can be readily prepared *via* oxidative coupling methods using $FeCl_3$ or $FeCl_3{\cdot}6H_2O$, and such methods are frequently employed.[60] However, the resulting polythiophenes, typically poly(3-hexylthiophene),[61,62] contain residual iron(III) salts, which are difficult to remove soley by washing with solvents and can only be removed through multiple washes with various solvents, followed by prolonged Soxhlet extractions with additional solvents. In the case of polypyrrole as well, it has been reported that ferric ions still remain after being washed with different solvents.[63] Furthermore, it has been reported that $FeCl_3$ can be doped into polyaniline.[64,65] Though the synthetic method developed herein is applicable only to conducting polymers that contain Fe^{3+} ions within their molecular structures, it may potentially be applicable to all major classes of conducting polymers since Fe^{3+} ions have been found to either remain within their structures during preparation, or could be externally introduced as stated above. Consequently, the current method has the potential to serve as a novel fabrication approach for diverse magnetic composite materials that show promise for application in both the biological and chemical fields.

Despite its potential, the current methodology is constrained by its applicability only to P3MeOT at present. Consequently, future research endeavors will aim to extend this technique to encompass not only other polythiophenes but also prominent conducting polymers, such as polypyrrole and polyaniline, with the objective of developing novel magnetic composite materials. Notably, when a conducting polymer is compatible with a solvent, it is feasible to form composites that can be dispersed within the solvent. These composites are well-suited for biomedical applications, including biosensors, drug delivery systems, and MRI contrast agents, owing to their superior biocompatibility and dispersion stability. Furthermore, given the potential to fabricate film coatings for electromagnetic shielding through the application of these dispersions, the formation of composites utilizing soluble conducting polymers will be prioritized in future research.

Author contributions

Katsuyoshi Hoshino: Conceptualization, formal analysis, funding acquisition, methodology, project administration, supervision, writing – original draft; Kiho Kashiwagi: Data curation, investigation, validation; Minako Tachiki: Data curation, investigation, methodology; Hyuma Masu: Investigation, validation, writing – review & editing; Satoru Tsukada: Funding acquisition, methodology, resources, supervision, validation, writing – review & editing.

Conflicts of interest

There are no conflicts to declare.

Data availability

The data that support the findings of this study have been included in the main text and supplementary information (SI). Supplementary information: elemental maps for P3MeOT-Cl, EDX measurements of P3MeOT-ClO_4 and Red 2, magnetism demonstrations for P3MeOT-ClO_4 and Red 2, XPS measurements for P3MeOT-ClO_4, XPS survey spectra of P3MeOT-Cl and Red 1, EDX spectra of P3MeOT-Cl and Red 1, and magnetic property measurements for Red 2 and P3MeOT-ClO_4. See DOI: https://doi.org/10.1039/d5py00933b.

Acknowledgements

The authors thank Prof. Masatomo Uehara of Yokohama National University for magnetic property measurements. We would also like to thank Editage (https://www.editage.jp) for English language editing.

References

1 Y. Tai, L. Wang, G. Yan, J.-M. Gao, H. Yu and L. Zhang, Recent Research Progress on the Preparation and Application of Magnetic Nanospheres, *Polym. Int.*, 2011, **60**, 976–994.
2 J. Thévenot, H. Oliveira and O. Sandre, S and Lecommandoux, Magnetic Responsive Polymer Composite Materials, *Chem. Soc. Rev.*, 2013, **42**, 7099–7116.
3 S. Kalia, S. Kango, A. Kumar, Y. Haldorai, B. Kumari and R. Kumar, Magnetic Polymer Nanocomposites for Environmental and Biomedical Applications, *Colloid Polym. Sci.*, 2014, **292**, 2025–2052.
4 K. Namsheer and C. S. Rout, Conducting Polymers: a Comprehensive Review on Recent Advances in Synthesis, Properties and Applications, *RSC Adv.*, 2021, **11**, 5659–5697.
5 Y. Kim and X. Zhao, Magnetic Soft Materials and Robots, *Chem. Rev.*, 2022, **122**, 5317–5364.
6 M. K. Goswami, A. Srivastava, R. K. Dohare, A. K. Tiwari and A. Srivastav, Recent Advances in Conducting Polymer-Based Magnetic Nanosorbents for Dyes and Heavy Metal Removal: Fabrication, Applications, and Perspective, *Environ. Sci. Pollut. Res.*, 2023, **30**, 73031–73060.
7 H. Gu, C. Ma, J. Gu, J. Guo, X. Yan, J. Huang, Q. Zhang and Z. Guo, An overview of multifunctional epoxy nanocomposites, *J. Mater. Chem. C*, 2016, **4**, 5890–5906.
8 A. G. Díez, N. Pereira, C. R. Tubio, J. L. Vilas-Vilela, C. M. Costa and S. Lanceros-Mendez, Magnetic Polymer Actuators with Self-Sensing Resistive Bending Response Based on Ternary Polymer Composites, *ACS Appl. Electron. Mater.*, 2023, **5**, 3426–3435.
9 B. Han, R. Wang, X. Wei and R. Gu, Facile Fabrication of Fe_3O_4/Polypyrrole/Functionalized Carbon Nanotubes Composites for Photocatalytic Degradation of Contaminants from Wastewater, *Int. J. Electrochem. Sci.*, 2021, **16**, 210715.

10 I. S. Elashmawi and H. M. Alhusaiki-Alghamdi, Fabrication, Characterization, Spectroscopic, and Magnetic Properties of Polyaniline/Magnetite (PANi/Fe_3O_4) Nanocomposites, *Opt. Quantum Electron.*, 2024, **56**, 1090.
11 M. D. Butterworth, S. P. Armes and A. W. Simpson, Synthesis of Poly(pyrrole)–Silica–Magnetite Nanocomposite Particles, *J. Chem. Soc., Chem. Commun.*, 1994, 2129–2130.
12 M. L. M. Elizalde, C. Acha, M. S. Moreno and P. S. Antonel, Tuning the Electrical and Magnetic Properties in Multifunctional Composite Materials Based on the PEDOT: DBS Conducting Polymer and Magnetite Nanoparticles, *J. Mater. Chem. C*, 2022, **10**, 18264–18278.
13 Z.-M. Zhang, Y. Wang, Q. Li, L.-M. Yu, J. Travas-Sejdicb and L. J. Zhang, Bowl-Shaped Poly(3,4-ethylenedioxythiophene)/ γ-Fe_2O_3 Composites with Elecromagnetic Function, *Chin. J. Polym. Sci.*, 2013, **31**, 503–513.
14 Y. Jin, X. Luo, J. Zhang, Y. Yu, J. An, J. Zhang, D. Zhao and K. Gao, Enhanced Electro-magnetic Wave Absorbing Properties of Fe_3O_4-Polyaniline Nano-Composites, *Sci. Adv. Mater.*, 2021, **13**, 938–943.
15 K. Singh, A. Ohlan, P. Saini and S. K. Dhawan, Poly (3,4-ethylenedioxythiophene) γ-Fe_2O_3 Polymer Composite–Super Paramagnetic Behavior and Variable Range Hopping 1D Conduction Mechanism – Synthesis and Characterization, *Polym. Adv. Technol.*, 2008, **19**, 229–236.
16 A. De, P. Sen, A. Poddar and A. Das, Synthesis, Characterization, Electrical Transport and Magnetic Properties of PEDOT–DBSA–Fe_3O_4 Conducting Nanocomposite, *Synth. Met.*, 2009, **159**, 1002–1007.
17 J. Deng, Y. Peng, C. He, X. Long, P. Li and A. S. C. Chan, Magnetic and Conducting Fe_3O_4-Polypyrrole Nanoparticles with Core-Shell Structure, *Polym. Int.*, 2003, **52**, 1182–1187.
18 J. Deng, C. He, Y. Peng, J. Wang, X. Long, P. Li and A. S. C. Chan, Magnetic and Conductive Fe_3O_4-Polyaniline Nanoparticles with Core–Shell Structure, *Synth. Met.*, 2003, **139**, 295–301.
19 M. Tachiki, R. Tagawa and K. Hoshino, Oligo(3-methoxythiophene)s as Water-Soluble Dyes for Highly Lustrous Gold- and Bronze-Like Metal-Effect Coatings and Printings, *ACS Omega*, 2020, **5**, 24379–24388.
20 M. Tachiki, S. Tsukada and K. Hoshino, Effect of Polymerization Rate on the Chemical and Optical Properties of Solution-Cast Metal-Like Lustrous Films of Water-Soluble 3-Methoxythiophene Oligomer Dyes, *Dyes Pigm.*, 2021, **190**, 109302.
21 R. Tagawa, H. Masu, T. Itoh and K. Hoshino, Solution-Cast Self-Assembled Films of Perchloratedoped Oligo(3-methoxythiophene) Showing a Gold-Like Luster, *RSC Adv.*, 2014, **4**, 24053–24058.
22 M. Kubo, H. Doi, R. Saito, K. Horikoshi, S. Tsukada and K. Hoshino, Effect of Polymerization Conditions on Physicochemical Properties of Gold-Like Lustrous Films of Organic Solvent Soluble 3-Methoxythiophene Oligomers, *Polym. J.*, 2021, **53**, 1019–1029.
23 Y. Takashina, T. Mitogawa, K. Saito and K. Hoshino, Chemical Events in Oligo(3-methoxythiophene) Coating Solutions and Their Effect on the Goldlike Coating Film Properties, *Langmuir*, 2018, **34**, 3049–3057.
24 D. Kelkar and A. Chourasia, Structural Properties of Polythiophene Doped with $FeCl_3$, *Chem. Chem. Technol.*, 2011, **5**, 309–315.
25 M. J. Winokur, P. Wamsley, J. Moulton, P. Smith and A. J. Heeger, Structural Evolution in Iodine-Doped Poly(3-alkylthiophenes), *Macromolecules*, 1991, **24**, 3812–3815.
26 E. A. Osborne, T. M. Atkins, D. A. Gilbert, S. M. Kauzlarich, K. Liu and A. Y. Louie, Rapid Microwave-Assisted Synthesis of Dextran-Coated Iron Oxide Nanoparticles for Magnetic Resonance Imaging, *Nanotechnology*, 2012, **23**, 215602.
27 Z.-M. Zhang, Y. Wang, Q. Li, L.-M. Yu, J. Travas-Sejdic and L. J. Zhang, Bowl-Shaped Poly(3,4-ethylenedioxythiophene)/ γ-Fe_2O_3 Composites with Elecromagnetic Function, *Chin. J. Polym. Sci.*, 2013, **31**, 503–513.
28 Y. I. Kim and W. E. Hatfield, Electrical, Magnetic and Spectroscopic Properties of Tetrathiafulvalene Charge Transfer Compounds with Iron, Ruthenium, Rhodium and Iridium Halides, *Inorg. Chim. Acta*, 1991, **188**, 15–24.
29 N. S. McIntyre and D. G. Zetaruk, X-ray Photoelectron Spectroscopic Studies of Iron Oxides, *Anal. Chem.*, 1977, **49**, 1521–1529.
30 B. J. Tan, K. J. Klabunde and P. M. A. Sherwood, X-ray Photoelectron Spectroscopy Studies of Solvated Metal Atom Dispersed Catalysts. Monometallic Iron and Bimetallic Iron-Cobalt Particles on Alumina, *Chem. Mater.*, 1990, **2**, 186–191.
31 M. Oku and K. Hirokawa, X-ray Photoelectron Spectroscopy of Co_3O_4, Fe_3O_4, Mn_3O_4 and Related Compounds, *J. Electron Spectrosc. Relat. Phenom.*, 1976, **8**, 475–481.
32 S. Majumder, M. Sardar, B. Satpati, S. Kumar and S. Banerjee, Magnetization Enhancement of Fe_3O_4 by Attaching onto Graphene Oxide: An Interfacial Effect, *J. Phys. Chem. C*, 2018, **122**, 21356–21365.
33 V. I. Nefedov, Y. V. Salyn, G. Leonhardt and R. Scheibe, A Comparison of different Spectrometers and Charge Corrections Used in X-Ray Photoelectron Spectroscopy, *J. Electron Spectrosc. Relat. Phenom.*, 1977, **10**, 121–124.
34 E. Paparazzo, XPS and Auger Spectroscopy Studies on Mixtures of the Oxides SiO_2, Al_2O_3, Fe_2O_3, and Cr_2O_3, *J. Electron Spectrosc. Relat. Phenom.*, 1987, **43**, 97–112.
35 A. P. Grosvenor, B. A. Kobe, M. C. Biesinger and N. S. McIntyre, Investigation of Multiplet Splitting of Fe 2p XPS Spectra and Bonding in Iron Compounds, *Surf. Interface Anal.*, 2004, **36**, 1564–1574.
36 Y. Momose, K. Tsuruya, T. Sakurai and K. Nakayama, Photoelectron Emission and XPS Studies of Real Iron Surfaces Subjected to Scratching in Air, Water, and Organic Liquids, *Surf. Interface Anal.*, 2016, **48**, 202–211.
37 R. M. T. Sanchez, E. M. Curt, C. Volzone, R. C. Mercader and A. L. Cavalieri, Study of Fe(II) Oxidation in Ground Magnetite, *Mater. Res. Bull.*, 1990, **25**, 553–561.

38 X.-M. Liu and Y.-S. Li, One-Step Facile Fabrication of Ag/γ-Fe_2O_3 Composite Microspheres, *Mater. Sci. Eng., C*, 2009, **29**, 1128–1132.
39 Y.-S. Lee, H.-T. Kim and K.-O. Yoo, Effect of Ferric Oxide on the High-Temperature Removal of Hydrogen Sulfide over ZnO-Fe_2O_3 Mixed Metal Oxide Sorbent, *Ind. Eng. Chem. Res.*, 1995, **34**, 1181–1188.
40 J. Yue and A. J. Epstein, XPS Study of Self-Doped Conducting Polyaniline and Parent Systems, *Macromolecules*, 1991, **24**, 4441–4445.
41 W.-W. Wang, Y.-J. Zhu and M.-L. Ruan, Microwave-Assisted Synthesis and Magnetic Property of Magnetite and Hematite Nanoparticles, *J. Nanopart. Res.*, 2007, **9**, 419–426.
42 D. Cantillo, M. Baghbanzadeh and C. O. Kappe, In Situ Generated Iron Oxide Nanocrystals as Efficient and Selective Catalysts for the Reduction of Nitroarenes using a Continuous Flow Method, *Angew. Chem., Int. Ed.*, 2012, **51**, 1–5.
43 H. Wiogo, M. Lim, P. Munroe and R. Amal, Understanding the Formation of Iron Oxide Nanoparticles with Acicular Structure from Iron(III) Chloride and Hydrazine Monohydrate, *Cryst. Growth Des.*, 2011, **11**, 1689–1696.
44 M. Sharma, A. Kumar, D. Sajwan, K. Kumari, B. P. Mishra and V. Krishnan, Photocatalysis for Sustainable Nitrogen Fixation: Fundamentals, Catalyst Design, Nanoarchitectonics, Applications, and Future Prospects, *Adv. Sustainable Syst.*, 2025, **9**, 2400903.
45 E. Villa, E. Agosti, C. Castiglioni, M. C. Gallazzi and G. Zerbi, Through Bond and Through Space Interactions in Oligo–Alkoxythiophenes: A Spectroscopic Study, *J. Chem. Phys.*, 1996, **105**, 9461–9469.
46 B. Dong, J. Xu, L. Zheng and J. Hou, Electrodeposition of Conductive Poly(3-methoxythiophene) in Ionic Liquid Microemulsions, *J. Electroanal. Chem.*, 2009, **628**, 60–66.
47 S. Tanaka, M. Sato and K. Kaeriyama, Electrochemical preparation and Properties of Poly(3-methoxy-2,5-Thiophenediyl) and Poly(3-Methylthio-2,5-thiophenediyl), *Synth. Met.*, 1988, **25**, 277–288.
48 D. Gningue-Sall, M. Fall, M. M. Dieng, J. J. Aaron and P. C. Lacaze, Electrosynthesis and Characterization of Poly (3-methoxythiophene)–Polybithiophene Composite Films Prepared in Micellar Media on Pt and Fe Substrates, *Phys. Chem. Chem. Phys.*, 1999, **1**, 1731–1734.
49 S. Tanaka, M. Sato and K. Kaeriyama, Electrochemical Polymerization of Thiophenes Containing a Methoxy Group, *Polym. Commun.*, 1985, **26**, 303–306.
50 S. Husain, M. Irfansyah, N. H. Haryanti, S. Suryajaya, S. Arjo and A. Maddu, Synthesis and Characterization of Fe_3O_4 Magnetic Nanoparticles from Iron Ore, *J. Phys.: Conf. Ser.*, 2019, **1242**, 012021.
51 M. Srivastava, J. Singh, M. Yashpal, D. K. Gupta, R. K. Mishra, S. Tripathi and A. K. Ojha, Synthesis of Superparamagnetic Bare Fe_3O_4 Nanostructures and Core/Shell (Fe_3O_4/Alginate) Nanocomposites, *Carbohydr. Polym.*, 2012, **89**, 821–829.
52 Y. Wei, B. Han, X. Hu, Y. Lin, X. Wang and X. Deng, Synthesis of Fe_3O_4 Nanoparticles and Their Magnetic Properties, *Procedia Eng.*, 2012, **27**, 632–637.
53 S. H. Chaki, T. J. Malek, M. D. Chaudhary, J. P. Tailor and M. P. Deshpande, Magnetite Fe_3O_4 Nanoparticles Synthesis by Wet Chemical Reduction and Their Characterization, *Adv. Nat. Sci.: Nanosci. Nanotechnol.*, 2015, **6**, 035009.
54 G. Tourillon, in *Handbook of Conducting Polymers*, ed. T. A. Skotheim, Marcel Dekker, New York and Basel, 1986, ch. 9, pp. 293–350.
55 H. El Ghandoor, H. M. Zidan, M. M. H. Khalil and M. I. M. Ismail, Synthesis and Some Physical Properties of Magnetite (Fe_3O_4) Nanoparticles, *Int. J. Electrochem. Sci.*, 2012, **7**, 5734–5745.
56 S. Si, C. Li, X. Wang, D. Yu, Q. Peng and Y. Li, Magnetic Monodisperse Fe_3O_4 Nanoparticles, *Cryst. Growth Des.*, 2005, **5**, 391–393.
57 R. Qiao, C. Fu, H. Forgham, I. Javed, X. Huang, J. Zhu, A. K. Whittaker and T. P. Davis, Magnetic Iron Oxide Nanoparticles for Brain Imaging and Drug Delivery, *Adv. Drug Delivery Rev.*, 2023, **197**, 114822.
58 C. L. Meiseli, P. Bainbridge, R. V. Mulkern, D. Mitsouras and J. Y. Wong, Assessment of Superparamagnetic Iron Oxide Nanoparticle Poly(Ethylene Glycol) Coatings on Magnetic Resonance Relaxation for Early Disease Detection, *IEEE Open J. Eng. Med. Biol.*, 2020, **1**, 116–122.
59 K. Wu, D. Su, J. Liu, R. Saha and J.-P. Wang, Magnetic Nanoparticles in Nanomedicine: a Review of Recent Advances, *Nanotechnology*, 2019, **30**, 502003.
60 R. Sugimoto, S. Takeda, H. B. Gu and K. Yoshino, Preparation of Soluble Polythiophene Derivatives Utilizing Transition Metal Halides as Catalysts and Their Property, *Chem. Express*, 1986, **1**, 635–638.
61 M. S. A. Abdou and S. Holdcroft, Mechanisms of Photodegradation of Poly(3-alkylthiophenes) in Solution, *Macromolecules*, 1993, **26**, 2954–2962.
62 M. S. A. Abdou, X. Lu, Z. W. Xie, F. Orfino, M. J. Deen and S. Holdcroft, Nature of Impurities in π-Conjugated Polymers Prepared by Ferric Chloride and Their Effect on the Electrical Properties of Metal-Insulator-Semiconductor Structures, *Chem. Mater.*, 1995, **7**, 631–641.
63 R. Agrawal, J. Shah, G. Gupta, R. Srivastava, C. Sharma and R. Kotnala, Significantly High Electromagnetic Shielding Effectiveness in Polypyrrole Synthesized by Eco-Friendly and Cost-Effective Technique, *J. Appl. Polym. Sci.*, 2020, **137**, e49566.
64 F. Genoud, I. Kulszewicz-Bajer, A. Bedel, L. J. Oddou, C. Jeandey and A. Pron, Lewis Acid Doped Polyaniline. Part II: Spectroscopic Studies of Emeraldine Base and Emeraldine Hydrochloride Complexation with $FeCl_3$, *Chem. Mater.*, 2000, **12**, 744–749.
65 I. Kulszewicz-Bajer and J. Suwalski, Mössbauer Spectroscopic Studies of Polyaniline Doped with $FeCl_3$, *Synth. Met.*, 1988, **25**, 277–288.

